Synthesis of Extra-Large Pore, Large Pore and Medium Pore Zeolites Using a Small Imidazolium Cation as the Organic Structure-Directing Agent

Zihao Rei Gao,[a] Salvador R. G. Balestra,[a] Jian Li,[b] and Miguel A. Camblor*[a]

Abstract: One common strategy in the search for new zeolites is the use of organic structure-directing agents (OSDA). Typically, one seeks to achieve a high specificity in the structure-directing effect of the OSDA. This study shows, however, that an OSDA lacking strong specificity towards any particular zeolite may provide opportunities for discovery when other synthesis parameters are systematically screened. Thus, 1-methyl-2-ethyl-3-*n*-propylimidazolium has allowed to crystallize the new large/medium pore zeolite HPM-16 as well as the recently reported extra-large pore **-SYT** and the medium/small pore and chiral **STW**. The sophisticated OSDA originally affording **-SYT** and the new simple OSDA have very little in common, both in terms of size, shape and flexibility, while both may still direct the synthesis of the same zeolite. In fact, molecular simulations show that the new OSDA is located in three different positions of the **-SYT** structure, including the discrete 8MR where the original organic could not fit.

Introduction

Since their first use in 1989,[1] imidazolium cations have been widely used in the synthesis of zeolites,[2–4] although new zeolite structures were not reported until 2003,[5] when imidazolium cations were combined with fluoride anions in concentrated conditions.[6] Compared to the aliphatic quaternary ammonium cations most frequently used as OSDAs in zeolite synthesis, imidazolium cations show large differences in molecular size and shape and charge distribution.[7,8] Imidazolium cations have allowed the synthesis of many new zeolites.[3] For instance, some small-sized imidazolium cations are good templates for several pure-silica zeolites, including **ITW**,[9] **STW**,[10,11] **RTH**,[12] or novel aluminosilicate zeolites, including **PWO** and **PWW**,[13,14] and PST-24.[15] Also, benzyl substituted imidazolium cations were used to discover several novel large and/or extra-large pore germanosilicate zeolites.[16–20] Moreover, dications featuring two linked imidazolium moieties separated by four carbon units are found to be good OSDAs for the chiral zeolite **STW**,[21] and when the OSDA is also chiral allows the preparation of the enantiomerically enriched zeolite.[22] Besides, since they may function as ionic liquids (IL), imidazoliums could also be used as both the OSDA and the solvent, in the so-called ionothermal synthesis, in order to get some known and new phosphate-based zeolites.[23–25]

Recently, we reported the synthesis of the novel zeolite HPM-16 by using another small-sized imidazolium cation, 1-methyl-2-ethyl-3-*n*-propylimidazolium (1M2E3nPrIM) as the OSDA.[26] Here we report a screening of synthesis conditions by using the same OSDA, and varying the Ge molar fraction (Ge_f = Ge/(Ge + Si)) and the water content in the synthesis mixture. Interestingly, three zeolites with very different pore apertures (as implied by the number of tetrahedra, MR, forming the smallest ring along the diffusional path) can be synthesized from the same OSDA: the extra-large pore interrupted zeolite **-SYT** (24 membered-ring, MR),[27] the large/medium pore zeolite HPM-16 (12 and 10 MR),[26] and the medium/small pore chiral zeolite **STW** (10 and 8 MR).[28] Combining the experimental results with calculations, the OSDA location within the channel of zeolite **-SYT** is also studied in this work, showing a quite distinct OSDA position compared with the original OSDA used to discover it.[27] For pure silica compositions mainly "default" structures[29] not very demanding of structure-direction specificity were obtained: **TON** at 175 °C, **STF** at 150 °C. Intriguingly, the addition of HPM-16 seeds lead to the crystallization of **MTW** (another default structure). But for aluminosilicate compositions we obtained **MEL**, a phase that we do not consider a default structure. The diversity of structures and pores of the zeolites obtained (some of them very recently reported for the first time) highlight the richness that can be achieved by screening the synthesis parameters using a "less specific" OSDA, for which the final product greatly depends on other, frequently subtle, conditions.[30–32]

[a] *Z. R. Gao, Dr. S. R. G. Balestra, Prof. Dr. M. A. Camblor*
Instituto de Ciencia de Materiales de Madrid
Consejo Superior de Investigaciones Científicas (ICMM–CSIC)
c/ Sor Juana Inés de la Cruz, 3, Madrid, 28049 (Spain)
E-mail: macamblor@icmm.csic.es

[b] *Dr. J. Li*
Berzelii Center EXSELENT on Porous Materials
Department of Materials and Environmental Chemistry
Stockholm University
Stockholm, 10691 (Sweden)

Supporting information for this article is available on the WWW under https://doi.org/10.1002/chem.202103288

Results and Discussion

Zeolite Synthesis

SYSU-3 (-**SYT**), containing an extra-large 24MR pore, was first reported by Jiang et al. in 2018 using a large aliphatic ammonium dication (N,N′-dimethylsophoridinium dication, Me_2SOP, Figure 1b) as the OSDA with $Ge_f = Ge/(Ge+Si) = 0.5$ in the synthesis mixture.[27] Me_2SOP is a derivative of a natural, scarce product and it was believed that its bulky nature and "unique skeleton" were determinant to the crystallization of the extra-large pore SYSU-3. In our work, however, a small, aromatic, easy-to-prepare OSDA, 1-methyl-2-ethyl-3-*n*-propylimidazolium cation, 1M2E3nPrIM (Figure 1a), derived from a commercial imidazole, was also successfully used to synthesize **-SYT** at a relatively lower Ge content ($Ge_f = 0.3$ in gel) under concentrated conditions ($H_2O/T = 2.5$; entry 4 in Table S1).

The crystallization area of **-SYT** is heavily influenced by the Ge_f in the synthesis mixture (Table S1). At a higher Ge_f (0.5), **-SYT** could still be successfully crystallized (entry 1). At a lower Ge_f (0.15; entry 18), an amorphous phase always remained together with **-SYT** in the product, even when the Ge_f and H_2O/T values were decreased at the same time (entries 17 and 22). The phase area is also narrow with respect to the H_2O/T value. At relatively high Ge_f (0.5 or 0.3), the H_2O/T value may be increased up to 5 to get **-SYT** with various amounts of amorphous phase (entries 2, 5) and this H_2O/T value is the highest that can be used to get **-SYT**. These trends are more clearly summarized in a phase diagram (Figure 2), where **-SYT** lies at the top left region (high concentration and high Ge_f).

HPM-16 could also be synthesized with the same OSDA at higher degrees of dilution and the best HPM-16 samples were prepared from gels of composition 0.7 SiO_2:0.3 GeO_2:0.5 OSDAOH:0.5 HF:10 H_2O at 160 °C for 6–9 days within a static autoclave (entries 7c–7f in Table S1). The structure elucidation, stabilization and a full characterization of HPM-16 were reported before.[26] When shortening or enlarging the crystallization time (3–5 or 13 days; entries 7a–7b or 7g, respectively), a trace of impurity also appeared. Because of the extremely tiny amount of the impurity, it was impossible to identify it from the powder X-ray diffraction (PXRD) patterns. When those gels were heated in rotated autoclaves (entries 8a–8d), a visible **STW** impurity always crystallized along with HPM-16. After a high-throughput series of experiments, we discovered that HPM-16 is very sensitive to the water content in the gel. At the same Ge_f used for HPM-16 (0.3), the products were **-SYT** (totally crystallized at $H_2O/T = 2.5$ and ill-crystallized at $H_2O/T = 5$; entries 4, 5 and Figure 3a, 3b), **STW** ($H_2O/T = 7.5$; entry 6 and Figure 3c), pure HPM-16 (H2O/T = 10; entry 7d and Figure 3d), a mixture of HPM-16 and a **CSV**-like phase ($H_2O/T = 13.5$; entry 9 and Figure 3e), and a mixture of HPM-16 and a possibly layered material ($H_2O/T = 15$; entry 10 and Figure 3f). Small changes in the water content in gel significantly influence the product (see Figure 3). For the **CSV**-like phase, due to the fact that only 3 peaks belonging to this phase could be found from lab PXRD data, it was also very difficult to identify the phase. However, after an extensive search in the International Zeolite Association (IZA) database,[33] we find likely it is germanosilicate zeolite **CSV**.[34] Besides, the Ge_f is also a key factor that heavily

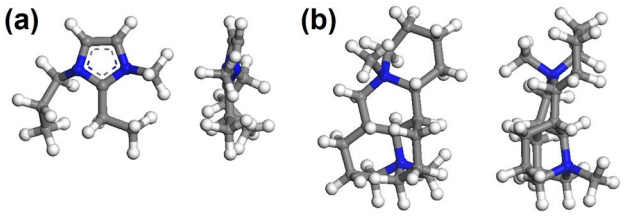

Figure 1. (a) The small and aromatic cationic OSDA (1M2E3nPrIM) used in this work, and (b) the large and aliphatic dicationic OSDA (Me_2SOP) used for the first reported **-SYT** zeolite synthesis. Atomic color: blue, grey, and white for N, C, and H, respectively.

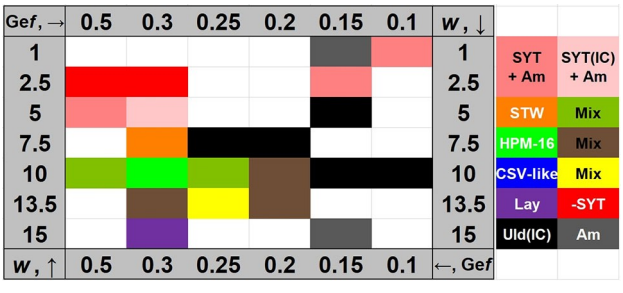

Figure 2. Synthetic product phase diagram from the OSDA 1M2E3nPrIM. The "mix" in color grass green, brown, and yellow correspond to mixtures of (**STW** + HPM-16), (HPM-16 + **CSV**-like phase), and (**STW** + HPM-16 + **CSV**-like phase), respectively. "Lay" refers to a likely layered phase while "Am", "IC", and "Uld" refer to amorphous, ill-crystallized and unidentified phases, respectively. We consider that a phase is ill-crystallized when all of its peaks are broad, while the presence of amorphous in a mixture is characterized by a broad reflection centered at around 22°.

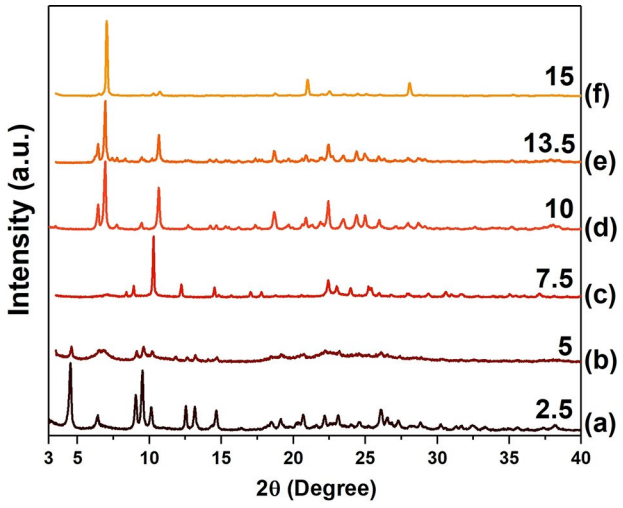

Figure 3. PXRD patterns of the synthesis results using OSDA 1M2E3nPrIM at $Ge_f = 0.3$ as a function of synthesis mixture concentration: (a) well crystallized **-SYT**, (b) amorphous-containing ill-crystallized **-SYT**, (c) **STW**, (d) pure HPM-16, (e) the mixture of HPM-16 and a **CSV**-like phase, (f) the mixture of HPM-16 and a likely layered material. The H_2O/TO_2 ratios in gels are given close to the curves.

Table 1. Determination of **-SYT** and **STW** framework composition.[a]

Zeolites (Lab Code)	Elemental Analysis Results N%	C%	H%	C/N	H/N	EDS Ge_f	Experimental Formula[d]	TG Weight Loss [%] 25–200 °C	200–800 °C
-SYT (ZG13004)	3.35	12.79	2.72	4.45 (4.5)[b]	11.29 (8.5)[b]	0.32 (0.3)[c]	$[Si_{87.0}Ge_{41.0}O_{248}(OH)_{16}] \mid (OSDAF)_{15.5}(H_2O)_{35.3}$	4.13 (4.90)[e]	20.18 (20.60)[f]
STW (ZG20901)	2.58	9.98	1.97	4.50 (4.5)[b]	10.59 (8.5)[b]	0.40 (0.3)[c]	$[Si_{36.0}Ge_{24.0}O_{120}] \mid (OSDAF)_{5.4}(H_2O)_{11.2}$	1.34 (3.47)[e]	16.49 (15.90)[f]

[a] Results for HPM-16 have been already published,[26] [b] Theoretical molar ratio in parenthesis, calculated from the OSDA formula, [c] Ge_f value in the synthesis mixture, [d] in this formula, OSDA = $C_9N_2H_{17}$ and the water content was determined from the excess H found, [e] expected water weight loss value, [f] expected OSDA fluoride weight loss value.

influenced the products. When Ge_f in gel ≥ 0.2, the competing phases are **STW** and the **CSV**-like phase (entries 3, 7d, 12, 15). With less Ge content in gel ($Ge_f \leq 0.15$), the products are always ill-crystallized solids. In Figure 2, **STW** and HPM-16 lie at the middle left area of the phase diagram (intermediate concentration and high Ge_f) and the mixture of HPM-16 and a **CSV**-like phase lies at the middle right area (intermediate concentration and low Ge_f). There is a large overlap region among those three phases resulting in mixtures, which lie in the center of the diagram.

Finally, synthesis without Ge was also studied and several "default structures", defined as stable zeolites that generally crystallize when the OSDA doesn't have a strong structure-direction effect,[29] were obtained by using this OSDA. At 175 °C, 160 °C, and 150 °C, **TON** (entries 24a–24d in Table S2), **MEL** (entries 27a–27b), and **STF** (entry 28), respectively, were prepared from a pure silica gel. With some HPM-16 seeds and also pure silica gel (seed/gel = 30%), the products at 160 °C are, intriguingly, mixtures of HPM-16 and **MTW** (entries 26a–26c). Apparently, the HPM-16 seeds are able to enhance the heteronucleation of **MTW** instead of its own homonucleation or crystal growth. Interestingly, with the addition of 2% $Al(OH)_3$, zeolite **MEL** crystallized at 175 °C from a fluoride-free gel (entries 25a–25d; morphology shown in Figure S1d). As opposed to the related **MFI**, we would not consider **MEL** as a certain default structure, following the definition given above.

Physicochemical Characterization

The **-SYT** zeolite synthesized by using OSDA 1M2E3nPrIM is a needle-like nanosized zeolite with less than 1 μm in length and a much smaller size in the other two dimensions (Figure S1b). The needles are assembled randomly into 5–50 μm aggregates (Figure S1a). The PXRD pattern of the as-synthesized material proved that this phase is the recently reported germanosilicate zeolite **-SYT** (Figure 3a) and the field emission scanning electron microscopy (FE-SEM) images proved that this sample is very pure without any amorphous phase or other particles with different morphologies. For the **STW** synthesized here, the crystals under FE-SEM are hexagonal bipyramids, with a size of 20 μm (Figure S1c). This is the most common morphology of germanosilicate **STW** zeolites with relatively large Ge_f,[28,35] while **STW** with lower germanium contents typically show also prismatic faces.[10,11] Energy-dispersive X-ray spectroscopy (EDS) tests showed the Ge_f in crystals of **-SYT**, HPM-16 and **STW** are 0.32, 0.30[26] and 0.40 (Table 1), respectively, indicating that the Ge_f in zeolite **-SYT** and HPM-16 are close to the Ge_f in the synthesis mixture (0.3), while this value in **STW** is a bit higher. The ^{29}Si magic angle spinning (MAS) NMR spectrum of as-made **-SYT** sample showed two featureless and broad peaks at −101.5 and −107.3 ppm (Figure S2), which is a typical ^{29}Si spectrum for an interrupted germanosilicate zeolite.[20] The ^{19}F MAS NMR spectrum of as-made **-SYT** sample showed 2 signals at −20.2 and −8.8 ppm (Figure 4), which correspond to F^- in d4r of types II and III, respectively,[35] very similar to the HPM-16 case,[26] but different from the previously reported **-SYT** material, which, due to its higher Ge content ($Ge_f = 0.5$ compared to 0.3 in our material), only displays type III resonances.[27] This demonstrates F is occluded exclusively in double 4-membered ring (d4r) of the **-SYT** phase.

To ensure that the true OSDA leading to the three different phases is the intact OSDA, we recorded ^1H and ^{13}C liquid NMR spectra of the as-made **-SYT**, HPM-16 and **STW** samples dissolved in a mixture of HF and D_2O. All the spectra (Figure 5b–5d for ^1H and Figure 6b-6d for ^{13}C NMR) match well with the OSDA bromide in D_2O (Figure 5a and Figure 6a), proving that the undecomposed OSDA could direct to the three different phases, even though the framework density value and

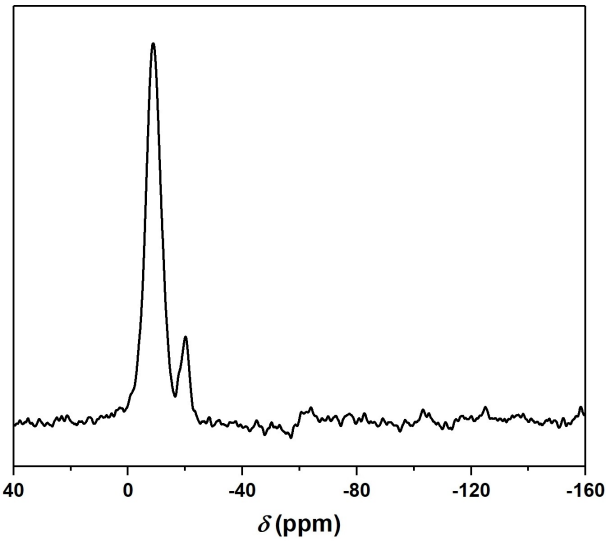

Figure 4. ^{19}F MAS NMR spectrum of as-made **-SYT** zeolite.

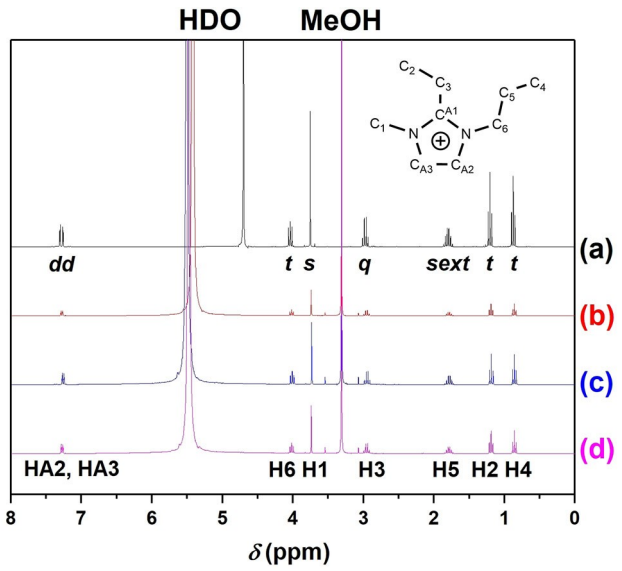

Figure 5. ^{1}H liquid NMR spectra of: (a) the OSDA 1M2E3nPrIM bromide in D_2O, and dissolved as-made samples in a mixture of HF and D_2O of (b) **-SYT** zeolite, (c) HPM-16, and (d) **STW** zeolite. All the proton resonances have been identified with their atom labels, corresponding to the molecular structure (inserted in the figure), and their respective splitting multiplicities are marked (*s*: singlet, *t*: triplet, *q*: quartet, *sext*: sextet, and *dd*: doublet of doublets). In (b–d), a drop of methanol was added as a chemical shift reference (3.31 ppm for the $C\underline{H}_3OH$). The resonance at 4.70 ppm in (a) and the resonances at 5.4–5.5 ppm in (b–d) are from HDO.

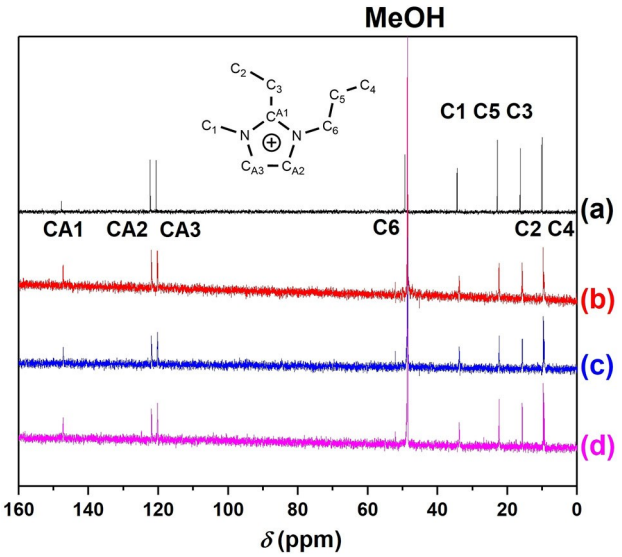

Figure 6. ^{13}C liquid NMR spectra of: (a) the OSDA 1M2E3nPrIM bromide in D_2O, and dissolved as-made samples in a mixture of HF and D_2O of (b) **-SYT** zeolite, (c) HPM-16, (d) **STW** zeolite. In (b–d), a drop of methanol was added as a chemical shift reference (48.6 ppm).

the channel system of these three structures are hugely different. By contrast, some decomposition of Me_2SOP was detected in the previous work on **-SYT**.[27] Chemical analysis of C, H, N also proved the integrity of the OSDA, showing about the same experimental and calculated C/N ratios (Table 1). Combining all the results, including the Ge_f in zeolites (via EDS), C, H, N elements contents and the structure information, the chemical formula of as-synthesized **-SYT** and **STW** could be determined as $[Si_{87.0}Ge_{41.0}O_{248}(OH)_{16}]\,|\,(OSDAF)_{15.5}(H_2O)_{35.3}$, and $[Si_{36.0}Ge_{24.0}O_{120}]\,|\,(OSDAF)_{5.4}(H_2O)_{11.2}$, respectively. Besides, the amount of water and OSDA agree reasonably with the low and high temperature losses in the thermogravimetric (TG) trace (Table 1 and Figures S3–S4). Small deviations in **STW** may be attributed to the presence of some amorphous material (Figure S1c).

The three main phases obtained with 1M2E3nPrIM are radically different. Zeolite **-SYT** is an interrupted extra-large pore zeolite with a channel system consisting of 3D intersecting 24×8×8 MR plus a 1D discrete 8MR (Figure 7a). The discrete 8MR channel does not connect with the extra-large 24MR channel, since its walls are made up of 4 and 6MR.[27] Zeolite HPM-16 is an interrupted large pore zeolite, also with a complex 3D intersecting 12+10×10(12)×12+10 MR channel (Figure 7b, 7c).[26] Zeolite **STW** is a true, fully-connected and chiral zeolite with 10MR and 8MR channel (Figure 7d).[10,11,28] The framework density calculated for the pure-silica polymorphs (FD_{Si}) of those three materials are 12.2, 15.2, 16.4, respectively.[26,33] Although the system seems to follow Villaescusa's Rule (i.e. denser zeolite phases tend to crystallize from synthesis mixtures with higher H_2O/TO_2 ratio values),[6] we note that the rule has been established for true zeolites, so its applicability to systems including interrupted frameworks (like **-SYT** and HPM-16) is so far uncertain.

The Fourier-transform infrared (FTIR) spectrum of **-SYT** in a self-supported wafer is shown in Figure 8. The presence of water in the as-made sample is characterized by a bending vibration band around 1631 cm^{-1}. After evacuation at 180 °C under vacuum, this band disappears while the OH stretching vibrations remain with a significant lower intensity and shifted to higher wavenumbers (around 3660 cm^{-1}), indicating that not very strong hydrogen bonds between the T–OH groups are established in the absence of water.

Calculations on -SYT

The 1M2E3nPrIM and Me_2SOP OSDAs exhibit several large differences between them with regard to aspects that have been argued to be of importance in structure-direction,[36] as illustrated in Figure 1 and Table 2. Despite these differences, both are able to produce **-SYT**, so we considered merited to study the OSDA preferential location and distribution within the channel of zeolite **-SYT** for 1M2E3nPrIM and Me_2SOP cations by molecular simulations.

The OSDA cations were firstly optimized using the GFN2-xTB basis set as implemented in the xTB (extended Tight Binding) v6.4.0 program package.[37,38] The atomic point charges were also calculated using this method. To compare the degree of flexibility between the two cations, we have calculated the ensemble of independent conformers for each cation using the CREST (v2.11) utility program.[39] We have identified the conformer ensembles using the automatized conformational search

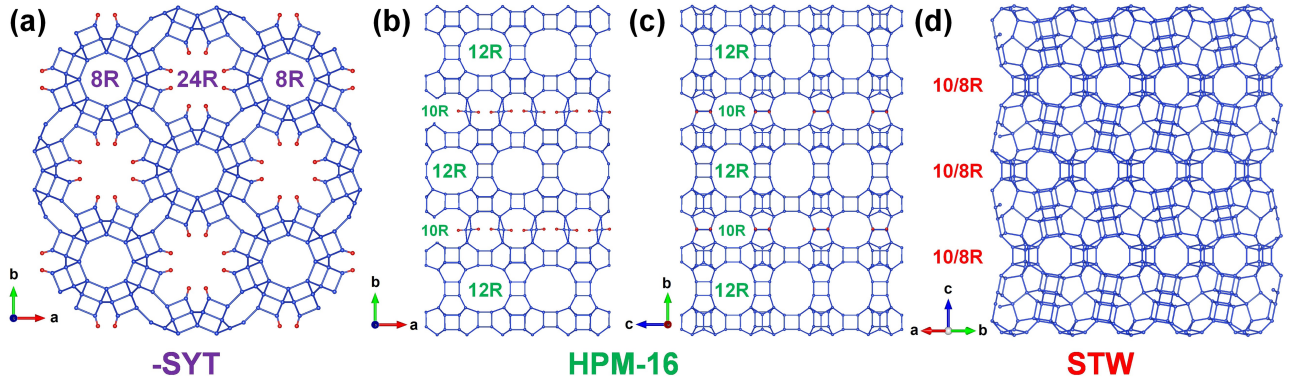

Figure 7. Structures of zeolite (a) **-SYT**, (b, c) HPM-16, and (d) **STW**. Only the T–T connections and the terminal T–O connections are shown.

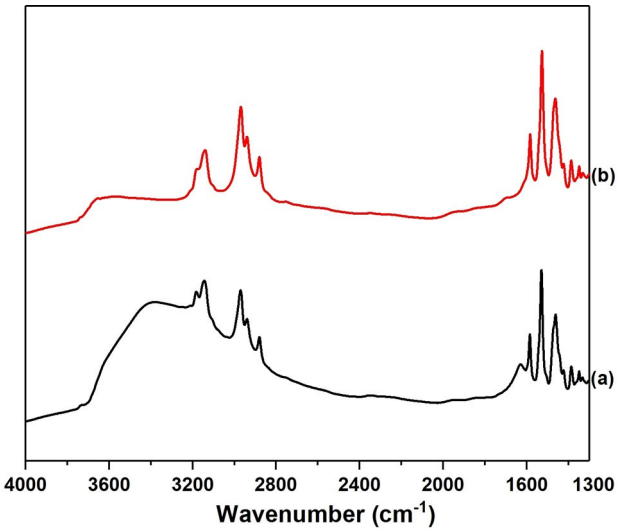

Figure 8. FTIR spectra of the self-supported pellet of **-SYT** zeolite (a) as-made and (b) dehydrated at 180 °C for 2 h under vacuum.

algorithm iMTD-GC.[40] The algorithm uses three descriptors to distinguish whether two configurations are conformers or rotamers: The potential energy difference between them, the rotational constants present in both molecules, and how much they overlap spatially with each other (by the root mean square deviation of their corresponding atomic positions). We have used the iMTD-GC algorithm as implemented in CREST, using an energy threshold of 10 kJ/mol, and leaving the rest of the parameters as default. We observe that the Me_2SOP dication is very rigid: The probability to choose a Me_2SOP in aqueous solution at 298.15 K matching the first most stable conformer is 0.983 of molar fraction or abundance in the whole ensemble (8 conformers). However, the 1M2E3nPrIM cation is much more flexible: Its most stable conformer has only a 0.145 abundance over the whole ensemble (14 conformers) in the same conditions of temperature and solvation. The ratio of abundance between the second and first conformers, a_2/a_1, are 0.976 and 0.014 for 1M2E3nPrIM and Me_2SOP, respectively, and indicates the degree of rigidity of the molecule. This implies 1M2E3nPrIM requires a flexible model, while Me_2SOP can be modelled as rigid. Regarding the model of the framework structure, random distributions of Ge ($Ge_f = 0.3$) generate compatible configurations with the ^{19}F NMR results (resonances II and III).[35] This can be explained by the fact that all T-sites belong to a d4r. The Q^3 atoms were terminated in hydroxyl groups, and a F^- anion was included per d4r. The bare structure was optimized following the same method we have recently used.[26]

We have performed the Monte Carlo simulations in the canonical ensemble (NVT MC) using the RASPA code, to insert the cations into the structure.[41] We have used the Dreiding forcefield for the intramolecular interactions of the cations,[42] plus TraPPE-zeo for the cross interatomic interactions between the framework, the extra-framework cations, and water.[43] This strategy was successfully employed in a previous study.[44] For water we have used the TIP4P-Ew model.[45] The amount of water in the structure for the synthesis with 1M2E3nPrIM is 35 molecules per unit cell. However, no mention about the amount of water in the structure was made in the work of Zhang et al. for the synthesis with Me_2SOP. To decide on a fixed number of molecules to be inserted into the structure for each composition in the NVT MC simulation, and to make the systems roughly comparable, we have proceeded as follows: Firstly, we

Table 2. Differences between two OSDAs able to produce **-SYT**.

OSDA	Chemical Formula	Connolly Volume [Å^3][a]	Charge	Chemical Nature	C/N	[(C + N)/ +][b]	3D Shape	Rigidity
Me_2SOP	$[C_{17}N_2H_{32}]^{2+}$	295	2+	Aliphatic	8.5	9.5	Bulky	High
1M2E3nPrIM	$[C_9N_2H_{17}]^{+}$	178	1+	Aromatic	4.5	11	Flat	Mixed[c]

[a] Calculated with a Connolly radius of 1 Å, [b] the ratio of (C + N)/charge, [c] large rigidity at the imidazolium ring and next C attached but large torsional freedom at the ethyl and propyl groups.

have done μVT MC simulations at very high pressure, 1×10^9 Pa, and 298 K as a reference state to calculate the water saturation uptake of the structure for each type of OSDA. It was 52 and 90 for 1M2E3nPrIM and Me_2SOP, respectively. Once we have calculated that, we compared with the experiments: for 1M2E3nPrIM there are 35 molecules of water, so this is ~70% of the saturation uptake capacity for SYSU-3. The corresponding 70% of water saturation uptake for Me_2SOP was 64 molecules per unit cell. Once the number of cations has been estimated, we proceed with the insertion with the NVT MC simulation. The fluoride anions were placed into the d4r cages and their movement out of the d4rs was prevented. Then, we performed 10^6 cycles in an NVT MC simulation to calculate the distribution of cations and water. Average occupation profiles in Figure 9a, 9b were obtained by using the software SITES-ANALYZER.[46,47]

We observed that 1M2E3nPrIM cations are distributed in three sites (Figure 9a): I) the interior of the tubular 8MR channel (*clo*-cages), and II) the pockets and III) around the center of the extra-large pore 24×8×8 MR channel system. In this case, 35 water molecules per unit cell are distributed solvating cations and bonded to the silanols forming weak hydrogen bonds. By contrast, the Me_2SOP are exclusively distributed around Site II, and the 8MR tubular channel systems are exclusively occupied by 45% of the water molecules (28 molecules). This is due to the small dimensions of the discrete 8MR pore and agrees with the previous work of Jiang et al.,[27] except that their model

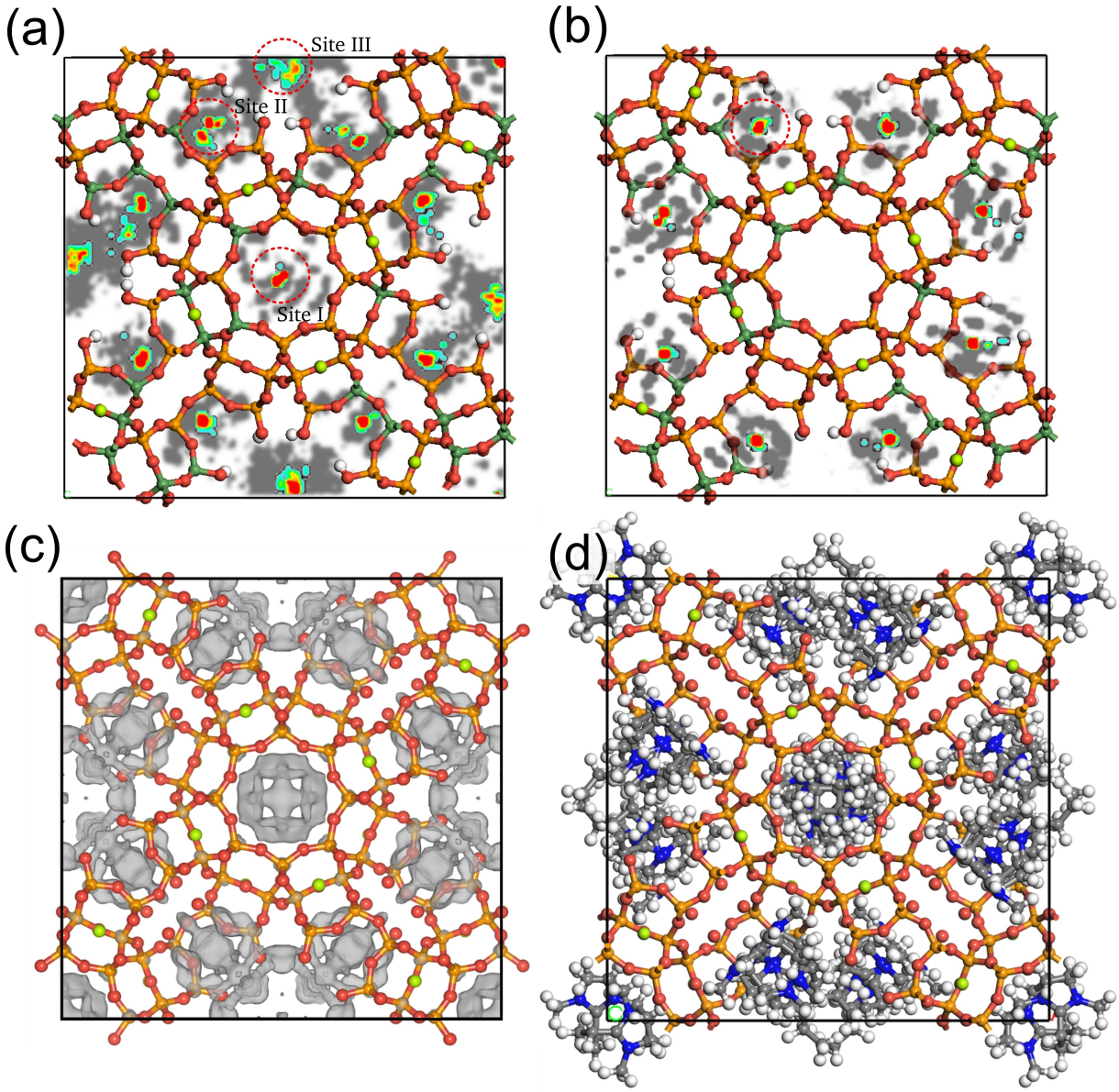

Figure 9. The location of cations in zeolite **-SYT**. Top: heatmap of the distribution of cations (1M2E3nPrIM and Me_2SOP, (a) and (b), respectively) found by molecular simulations. The gray heatmap is the average all-atom profile for OSDAs and the colored scale heatmap represents the average center-of-masses profile for OSDAs. Bottom: retrieved electron density from synchrotron PXRD (c) and disordered cation distribution determined by Rietveld refinement (d) for **-SYT** synthesized with 1M2E3nPrIM. Please note that the calculations are done with no symmetry, while the refinement is done in space group *I*4/*mcm*. Atomic color yellow, dark green, red, light green, blue, gray and white for Si, Ge, O, F, N, C and H atoms, respectively.

includes fluoride anions instead of water molecules occupying the 8MR channel in **-SYT**. Since it is very difficult to distinguish F^- and H_2O by X-ray diffraction (specially when fractional occupancies are used for F in both d4r and 8MR pores), we suggest a reevaluation of the original **-SYT** structure may be merited. In fact, a model with full occupancy of d4r by fluoride while water fills the 8MR discrete pores may agree better with the reported low temperature TG weight loss of 3%.[27] Similarly to the case with 1M2E3nPrIM, the rest of the water molecules (i.e. 35 water per unit cell), are solvating the OSDAs or bonded with the hydroxyl groups too. Thus, the smaller size of 1M2E3nPrIM and its flexibility given by the aliphatic branching allow it to adapt to all three cation site environments, as opposed to Me_2SOP.

Rietveld Refinement

In order to confirm the position of the guest molecule in **-SYT**, the method of combining simulated annealing and Rietveld refinement was used to locate 1M2E3nPrIM in the channels of **-SYT** by using high-resolution synchrotron PXRD. The detailed procedure has already been described in previous works.[48] During the Rietveld refinement process, the disordered 1M2E3nPrIM in **-STY** settled on the three independent sites: two of them located at the pockets and around the center of the 24MR channel and the third one located on the tubular individual 8MR channel, which matched well with the results of calculations. The refined occupancy of the OSDA atoms indicate a loading of 15.36 OSDA/uc, in good agreement with chemical analysis and TG results (Table 1). In addition, the retrieved residual electron density inside the channel system from synchrotron PXRD (Figure 9c, 9d) are close to the heatmap based on calculations (Figure 9a). At the final stage of Rietveld refinement, one water molecule with full occupancy (32 water per unit cell, also close to the observed value of 35.3) were included to refine close to the intersected 8MR channel, which resulted in the agreement factor $R_{wp}=5.32\%$, $R_p=3.38\%$. The refinement details are shown in Figure 10 and Tables S3–S5.

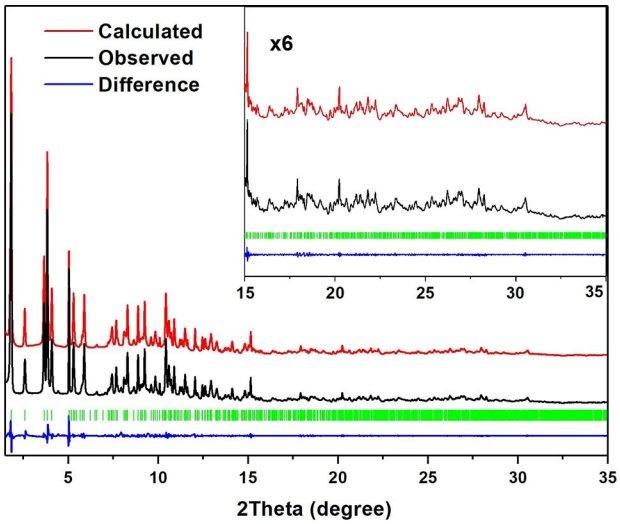

Figure 10. Rietveld refinement plot of as-synthesized **-SYT** ($\lambda=0.618668$ Å). Black, red and blue curves for experimental, calculated, and difference values, respectively. The vertical green lines mark the position of allowed reflections for zeolite **-SYT**.

Conclusion

In conclusion, the small-sized 1-methyl-2-ethyl-3-*n*-propylimidazolium cation was used as the OSDA in zeolite synthesis. Three zeolites **-SYT**, HPM-16 and **STW** were obtained in pure form from the germanosilicate system and several zeolite structures including **TON**, **MEL**, **MTW**, and **STF** were obtained from the (alumino)silicate system. The 24MR extra-large pore zeolite **-SYT** was characterized and studied, concluding that the OSDA was intact within the framework of **-SYT**, as it also occurs in HPM-16 and **STW** prepared from the same OSDA. Compared with Me_2SOP that was first reported in the synthesis of zeolite **-SYT**, our OSDA here shows a huge difference at the molecular level, and also in its position within the zeolite **-SYT**. The calculation study of the host-guest inorganic-organic interactions between zeolite **-SYT** and 1M2E3nPrIM was performed and discussed, showing the novel OSDA location in both sets of channels in zeolite **-SYT** in contrast to the original Me_2SOP, which cannot fit in the 8MR discrete pores. Those results were confirmed by Rietveld refinement. This work shows that OSDAs that show a little specificity in structure direction may provide a richness of zeolite structures and an opportunity for discovery, as shown here by the synthesis of the new HPM-16 (2021)[26] and the very recently reported **-SYT** (2018)[27] together with **STW** (2008).[28] This emphasizes S. B. Hong's idea that modification of the inorganic components or concentrations in synthesis carried out with flexible, hence unspecific OSDAs, may be an alternative strategy for the discovery of new zeolites,[30–32,49–51] extending it here to not such flexible OSDAs.

Experimental Section

The detailed information on the OSDA preparation was reported in a previous publication.[26] All the experimental entries in Tables S1–S2 follow the same basic synthesis procedure and two examples of products (zeolites **-SYT** and **STW**) are shown below for clarification. The detailed synthesis of HPM-16 has been reported elsewhere.[26]

Synthesis of zeolite -SYT: zeolite **-SYT** was synthesized from a gel of composition 0.3 GeO_2:0.7 SiO_2:0.5 OSDAOH:0.5 HF:2.5 H_2O at 160 °C for 7 days within a static autoclave (entry 4 in Table S1). 0.15666 g (1.50 mmol) of GeO_2 was firstly dissolved into 8.3088 g (2.55 mmol) of a 1M2E3nPrIM hydroxide solution with $[OH^-]=0.3075$ mmol/L. After complete hydrolyzation of the GeO_2, 785 μL (3.52 mmol) of tetraethylorthosilicate (TEOS) was added and hydrolyzed allowing to evaporate the ethanol produced and additional water, until the H_2O/TO_2 ratio target is reached (monitored by weight). Then, 95 μL (2.51 mmol) of titrated HF (26.45 mol/L) was added into the solution and the gel was transferred into a 30-mL Teflon insert in a steel autoclave. After crystallization at 160 °C for 7 days without rotation, the solid was filtrated and washed with water (30 mL×2) and acetone (30 mL×1), and then dried in the

oven overnight to get the product (0.341 g; yield: 32.8 g per 100 g of gel).

Synthesis of zeolite STW: zeolite **STW** was synthesized with the same OSDA from a gel of composition 0.3 GeO_2:0.7 SiO_2:0.5 OSDAOH:0.5 HF:7.5 H_2O at 160 °C for 7 days, also within a static autoclave (entry 6 in Table S1). To do so, 0.09434 g (0.902 mmol) of GeO_2 was dissolved into 4.8724 g (1.50 mmol) of a 1M2E3nPrIM hydroxide solution with $[OH^-]=0.3075$ mmol/L and the whole content was stirred until the solution became clear. Next, 465 μL (2.08 mmol) of TEOS was added, followed by addition of 57 μL (1.51 mmol) of HF ([HF] = 26.45 mol/L) after the water amount target is reached. The crystallization and solid handling were done as above to get **STW** (0.180 g; yield: 20.5 %).

Characterization methods: In order to observe the crystal morphology and to determine the Ge_f value in crystals, FE-SEM images and EDS data were collected on a FEI Nova NanoSEM 230 machine. For phase identification, PXRD patterns were recorded on a Bruker D8 Advance diffractometer ($\lambda = 1.5418$ Å, Cu Kα). Synchrotron PXRD data was collected at beamline BL04 (MSPD) in ALBA, the Spanish synchrotron radiation facility, in Debye-Scherrer mode ($\lambda =$ 0.618668 Å). To know the organic amount in the as-made zeolite sample, CHN elemental analysis was conducted by a LECO CHNS-932 analyzer. Also, TG analysis was conducted on an SDT Q600 TA instrument with a 100 mL/min air flow from 25 to 1000 °C with a 10 °C min^{-1} heating speed. Liquid NMR spectra were collected on a Bruker Avance III-HD Nanobay 300 MHz machine. Solid state MAS NMR spectra (^{13}C, ^{19}F, and ^{29}Si) were carried on a Bruker AV-400-WB equipment and the details have been given elsewhere.[9] For the HF dissolution experiment of the as-made zeolites, the method was reported in a previous work.[52] For the PXRD data collection with a cover of plastic film (Figure S5), the details were reported previously.[20]

Acknowledgements

This article is part of project PID2019-105479RB-I00 funded by MCIN/ AEI /10.13039/501100011033). SRGB was supported by grant FJC2018-035697-I funded by MCIN/AEI/10.13039/501100011033. Synchrotron experiments were performed at the Spanish ALBA Synchrotron with the collaboration of ALBA staff, and special thanks are due to A. Manjón. Centro Técnico Informático-CSIC, Trueno cluster facility of SGAI-CSIC is acknowledged for running the calculations. We also deeply thank C. Márquez-Álvarez for his kind help in characterization.

Conflict of Interest

The authors declare no conflict of interest.

Keywords: host-guest chemistry · hydrothermal synthesis · imidazolium · structure-directing agents · zeolites

[1] S. I. Zones, *Zeolites* **1989**, *9*, 458–467.
[2] P. Lu, L. A. Villaescusa, M. A. Camblor, *Chem. Rec.* **2018**, *18*, 713–723.
[3] L. Gómez-Hortigüela, M. A. Camblor, *Struct. Bond.* **2018**, *175*, 1–42.
[4] J. Shin, D. Jo, S. B. Hong, *Acc. Chem. Res.* **2019**, *52*, 1419–1427.
[5] P. A. Barrett, T. Boix, M. Puche, D. H. Olson, E. Jordan, H. Koller, M. A. Camblor, *Chem. Commun.* **2003**, 2114–2115.
[6] M. A. Camblor, L. A. Villaescusa, M. J. Díaz-Cabañas, *Top. Catal.* **1999**, *9*, 59–76.
[7] J. E. Schmidt, M. W. Deem, M. E. Davis, *Angew. Chem. Int. Ed.* **2014**, *53*, 8372–8374; *Angew. Chem.* **2014**, *126*, 8512–8514.
[8] D. Jo, S. B. Hong, *Chem. Commun.* **2018**, *54*, 487–490.
[9] A. Rojas, E. Martinez-Morales, C. M. Zicovich-Wilson, M. A. Camblor, *J. Am. Chem. Soc.* **2012**, *134*, 2255–2263.
[10] A. Rojas, M. A. Camblor, *Angew. Chem. Int. Ed.* **2012**, *51*, 3854–3856; *Angew. Chem.* **2012**, *124*, 3920–3922.
[11] A. Rojas, O. Arteaga, B. Kahr, M. A. Camblor, *J. Am. Chem. Soc.* **2013**, *135*, 11975–11984.
[12] J. E. Schmidt, M. A. Deimund, D. Xie, M. E. Davis, *Chem. Mater.* **2015**, *27*, 3756–3762.
[13] D. Jo, G. T. Park, J. Shin, S. B. Hong, *Angew. Chem. Int. Ed.* **2018**, *57*, 2199–2203; *Angew. Chem.* **2018**, *130*, 2221–2225.
[14] D. Jo, S. B. Hong, *Angew. Chem. Int. Ed.* **2019**, *58*, 13845–13848; *Angew. Chem.* **2019**, *131*, 13983–13986.
[15] D. Jo, J. Zhao, J. Cho, J. H. Lee, Y. Liu, C. Liu, X. Zou, S. B. Hong, *Angew. Chem. Int. Ed.* **2020**, *59*, 17691–17696; *Angew. Chem.* **2020**, *132*, 17844–17849.
[16] F.-J. Chen, Y. Xu, H.-B. Du, *Angew. Chem. Int. Ed.* **2014**, *53*, 9592–9596; *Angew. Chem.* **2014**, *126*, 9746–9750.
[17] J. H. Kang, D. Xie, S. I. Zones, S. Smeets, L. B. McCusker, M. E. Davis, *Chem. Mater.* **2016**, *28*, 6250–6259.
[18] Z.-H. Gao, F.-J. Chen, L. Xu, L. Sun, Y. Xu, H.-B. Du, *Chem. Eur. J.* **2016**, *22*, 14367–14372.
[19] F.-J. Chen, Z. R. Gao, J. Li, L. Gomez-Hortiguela, C. Lin, L. Xu, H.-B. Du, C. Marquez-Alvarez, J. Sun, M. A. Camblor, *Chem. Commun.* **2021**, *57*, 191–194.
[20] Z. R. Gao, J. Li, C. Lin, A. Mayoral, J. Sun, M. A. Camblor, *Angew. Chem. Int. Ed.* **2021**, *60*, 3438–3442; *Angew. Chem.* **2021**, *133*, 3480–3484.
[21] P. Lu, L. Gomez-Hortiguela, L. Xu, M. A. Camblor, *J. Mater. Chem. A* **2018**, *6*, 1485–1495.
[22] S. K. Brand, J. E. Schmidt, M. W. Deem, F. Daeyaert, Y. Ma, O. Terasaki, M. Orazov, M. E. Davis, *Proc. Nat. Acad. Sci. USA* **2017**, *114*, 5101–5106.
[23] E. R. Cooper, C. D. Andrews, P. S. Wheatley, P. B. Webb, P. Wormald, R. E. Morris, *Nature* **2004**, *430, 7003*, 1012–1016.
[24] E. R. Parnham, P. S. Wheatley, R. E. Morris, *Chem. Commun.* **2006**, *4*, 380–382.
[25] E. R. Parnham, R. E. Morris, *J. Am. Chem. Soc.* **2006**, *128*, 2204–2205.
[26] Z. R. Gao, S. R. G. Balestra, J. Li, M. A. Camblor, *Angew. Chem. Int. Ed.* **2021**, *60*, 20249–20252; *Angew. Chem.* **2021**, *133*, 20411–20414.
[27] C. Zhang, E. Kapaca, J. Li, Y. Liu, X. Yi, A. Zheng, X. Zou, J. Jiang, J. Yu, *Angew. Chem. Int. Ed.* **2018**, *57*, 6486–6490; *Angew. Chem.* **2018**, *130*, 6596–6600.
[28] L. Tang, L. Shi, C. Bonneau, J. Sun, H. Yue, A. Ojuva, B.-L. Lee, M. Kritikos, R. G. Bell, Z. Bacsik, J. Mink, X. Zou, *Nat. Mater.* **2008**, *7*, 381–385.
[29] A. Moini, K. D. Schmitt, E. W. Valyoscik, R. F. Polomski, *Zeolites* **1994**, *14*, 504–511.
[30] S.-H. Lee, D.-K. Lee, C.-H. Shin, Y.-K. Park, P. A. Wright, W. M. Lee, S. B. Hong, *J. Catal.* **2003**, *215*, 151–170.
[31] S. B. Hong, H.-K. Min, C.-H. Shin, P. A. Cox, S. J. Warrender, P. A. Wright, *J. Am. Chem. Soc.* **2007**, *129*, 10870–10885.
[32] S. B. Hong, *Catal. Surv. Asia* **2008**, *12*, 131–144.
[33] C. Baerlocher, L. B. McCusker, *Database of Zeolite Structures*: http://www.iza-structure.org/databases/, accessed on July. 29th, **2021**.
[34] J. E. Schmidt, D. Xie, T. Rea, M. E. Davis, *Chem. Sci.* **2015**, *6*, 1728–1734.
[35] R. T. Rigo, S. R. G. Balestra, S. Hamad, R. Bueno-Perez, A. R. Ruiz-Salvador, S. Calero, M. A. Camblor, *J. Mater. Chem. A* **2018**, *6*, 15110–15122.
[36] R. F. Lobo, S. I. Zones, M. E. Davis, *J. Inclusion Phenom. Mol. Recognit. Chem.* **1995**, *21*, 47–78.
[37] C. Bannwarth, S. Ehlert, S. Grimme, *J. Chem. Theory Comput.* **2019**, *15*, 1652–1671.
[38] C. Bannwarth, E. Caldeweyher, S. Ehlert, A. Hansen, P. Pracht, J. Seibert, S. Spicher, S. Grimme, *WIREs Comput. Mol. Sci.* **2021**, *11*, e1493.
[39] P. Pracht, F. Bohle, S. Grimme, *Phys. Chem. Chem. Phys.* **2020**, *22*, 7169–7192.
[40] S. Grimme, *J. Chem. Theory Comput.* **2019**, *15*, 2847–2862.
[41] D. Dubbeldam, S. Calero, D. E. Ellis, R. Q. Snurr, *Mol. Simul.* **2016**, *42*, 81–101.
[42] S. L. Mayo, B. D. Olafson, W. A. Goddard, *J. Phys. Chem.* **1990**, *94*, 8897–8909.
[43] P. Bai, M. Tsapatsis, J. I. Siepmann, *J. Phys. Chem. C* **2013**, *117*, 24375–24387.

[44] R. Bueno-Perez, S. R. G. Balestra, M. A. Camblor, J. G. Min, S. B. Hong, P. J. Merkling, S. Calero, *Chem. Eur. J.* **2018**, *24*, 4121–4132.
[45] H. W. Horn, W. C. Swope, J. W. Pitera, *J. Chem. Phys.* **2004**, *120*, 9665–9678.
[46] A. Sławek, J. M. Vicent-Luna, B. Marszałek, W. Makowski, S. Calero, *J. Phys. Chem. C* **2017**, *121*, 19226–19238.
[47] M. Vicent-Luna, *Sites-analyzer*: https://github.com/jmviclun/SITES-ANALYZER, **2017**.
[48] S. Smeets, L. B. McCusker, C. Baerlocher, S. Elomari, D. Xie, S. I. Zones, *J. Am. Chem. Soc.* **2016**, *138*, 7099–7106.
[49] S.-H. Lee, C.-H. Shin, D.-K. Yang, S.-D. Ahn, I.-S. Nam, S. B. Hong, *Microporous Mesoporous Mater.* **2004**, *68*, 97–104.
[50] J. Shin, S. B. Hong, *Microporous Mesoporous Mater.* **2009**, *124*, 227–231.
[51] S.-H. Lee, C.-H. Shin, G. J. Choi, T.-J. Park, I.-S. Nam, B. Han, S. B. Hong, *Microporous Mesoporous Mater.* **2003**, *60*, 237–249.
[52] P. Lu, L. Gomez-Hortiguela, Z. Gao, M. A. Camblor, *Dalton Trans.* **2019**, *48*, 17752–17762.

Manuscript received: September 10, 2021
Accepted manuscript online: November 3, 2021
Version of record online: November 17, 2021

